Journal of Catalysis 281 (2011) 279–289

Contents lists available at ScienceDirect

Journal of Catalysis

journal homepage: www.elsevier.com/locate/jcat

The effect of heat treatment on phase formation of copper manganese oxide: Influence on catalytic activity for ambient temperature carbon monoxide oxidation

Simon A. Kondrat [a], Thomas E. Davies [a], Zhongling Zu [b], Paul Boldrin [b], Jonathan K. Bartley [a], Albert F. Carley [a], Stuart H. Taylor [a], Matthew J. Rosseinsky [b], Graham J. Hutchings [a,*]

[a] Cardiff Catalysis Institute, School of Chemistry, Cardiff University, Main Building, Park Place, Cardiff CF10 3AT, UK
[b] Department of Chemistry, Crown Street, University of Liverpool, Liverpool L69 7ZD, UK

ARTICLE INFO

Article history:
Received 7 March 2011
Revised 8 May 2011
Accepted 10 May 2011
Available online 17 June 2011

Keywords:
Hopcalite
Copper manganese oxide
CO oxidation
Acetate decomposition

ABSTRACT

The auto-reduction of copper and manganese acetates has been investigated using *in situ* X-ray diffraction and thermogravimetric analysis, with the intention of manipulating the phenomena to tailor specific phase formation for synthesising catalysts. Subsequently catalysts prepared in this controlled manner were evaluated for ambient temperature CO oxidation. The decomposition of mixed copper and manganese acetate systems was controlled to form MnO_x-supported Cu or $CuMnO_x$ spinel structures, depending on the oxygen concentration and flow conditions during the heat treatment. Catalyst precursors were prepared by physical grinding and by a supercritical CO_2 anti-solvent precipitation process. The use of supercritical anti-solvent precipitation allows for the formation of well-mixed metal acetates that decompose to form active spinel CO-oxidation catalysts or small copper nano-particles supported on MnO_x, depending on the oxygen content of the heat treatment atmosphere. The ability to tune oxidation state and phase composition of catalysts is a key preparation parameter for controlling the activity and provides insight into the active sites for CO oxidation.

1. Introduction

Research in the field of metal oxide systems has immense importance in many areas of scientific study and applied technology. One such example is the Cu–Mn–O system, referred to as Hopcalite, which is an effective catalyst for a range of reactions, including ambient temperature CO oxidation, water gas shift reactions, complete oxidation of ethene and high temperature oxidation of volatile organic compounds [1–4]. Conventionally Hopcalite is prepared from metal nitrate salts, using co-precipitation or by physical mixing of the oxides [5,6]. Due to the environmental impact of nitrate waste streams and the high global warming potential of NO_x produced by conventional techniques, the use of alternative metal salts and precipitation techniques has recently been considered.

Our previous work concerning the precipitation of Hopcalite precursors using supercritical anti-solvent (SAS) CO_2 techniques has focused on the use of metal acetate salts [7]. The precursor material to the active $CuMnO_x$ CO oxidation catalyst was a well-mixed copper and manganese acetate. This was subsequently heat treated using a relatively standard calcination procedure in air to form the active catalyst.

The thermal decomposition of individual metal acetate salts has been extensively investigated by thermo-gravimetric analysis [8–10], as well as in line FT-IR and *in situ* X-ray diffraction (XRD) [11]. It has been concluded that for easily reducible metals such as copper, nickel and cobalt the acetate decomposition, in an oxygen free atmosphere, results in the autogenous reduction to the metal. In the case of less reducible elements such as manganese, zinc and iron, metal oxides are consistently formed [12]. The decomposition of the acetate complex typically starts with melting and subsequent dehydration of the materials with evolved gas analysis showing the formation of acetic acid during this initial stage. Acetic acid is considered to arise from the partial hydrolysis of the acetate complex [9]. The stages of acetate decomposition have been suggested by Pol and co-workers [12] to proceed as follows:

$$M(CH_3COO)_2 \rightarrow MCO_3 + CH_3COCH_3 \quad (1)$$

$$MCO_3 \rightarrow MO + CO_2 \quad (2)$$

$$CH_3COCH_3 \rightarrow CO + C_2H_6 \quad (3)$$

$$MO + CO \rightarrow M + CO_2 \quad (4)$$

It is known that the acetate decomposes into acetone and metal carbonate (Eq. (1)), which further decompose to CO and metal oxide, respectively (Eqs. (2) and (3)). The evolved CO facilitates

* Corresponding author.
E-mail address: hutch@cardiff.ac.uk (G.J. Hutchings).

0021-9517/$ - see front matter © 2011 Elsevier Inc. All rights reserved.
doi:10.1016/j.jcat.2011.05.012

the total reduction of certain metals such as copper (Eq. (4)), but not metals with a lower reduction potential such as iron. The decomposition is considered complex with other products including acetic acid and methane being produced. Judd et al. observed that acetic acid was the primary component when a metal is formed; whereas, acetone is the primary component for decomposition that results in metal oxides [8]. A kinetic study of the decomposition of nickel acetate by Leicester and Redman [13], which is in agreement with the mechanism suggested by Pol et al. [12], showed that rates of decomposition are affected by sample mass, due to a blanket of dense acetic acid formed from initial decomposition coating the sample.

This auto-reduction *via* heat treatment has previously been applied to the formation of individual metal particles on carbon nano-tube supports, prepared by physical mixing [14]. This included the use of the following metal acetates; Co, Cu, Au, Ag, Pd, Pt and Pb. In addition to this, both unsupported copper and nickel acetates have been reduced in reactant streams to the metal and tested for methanol reforming and cracking of methane respectively [15,16]. To the best of the authors' knowledge there have been no attempts to investigate or utilise the auto-reduction phenomena of mixed metal acetates in a beneficial manner for catalyst preparation, and hence this approach forms the basis of this study.

In this paper the effect of the decomposition of copper and manganese acetates on the formation of the spinel Hopcalite phase has been systematically investigated. The effect of oxygen content in the heat treatment atmosphere of copper and copper/manganese acetate mixtures has been investigated using *in situ* XRD analysis: scanning a narrow and targeted angle range has allowed for a high time "resolution" tracking of the metal oxide and metal phases observed during auto-reduction. This method far exceeds previous *in situ* XRD work that has principally highlighted dehydration and the final metal formation [11]. This technique has then been utilised in the investigation of physically mixed and intimately mixed copper and manganese systems produced by supercritical anti-solvent precipitation. The investigation of the physically mixed materials provides a model system with easily interpretable diffraction patterns, while auto-reduction of the intimately mixed precipitated material provides information on a practical system with potential catalytic uses. The differences in phase formation between these two mixing techniques illustrate the potential for controlling the solid state chemistry of well-mixed metal salt precursors with subsequent stabilisation of small discrete nanoparticles.

The set of materials produced by the range of heat treatment conditions were tested for ambient CO-oxidation. Heat treatment under variable oxygen containing atmospheres has been used to control Cu^{+}/Cu^{2+} ratios in the Hopcalite, and also to control the relative mixtures of the discrete metal oxides and mixed oxide phases. This approach allowed the study of the effect of copper and manganese phases and oxidation states on the activity for CO-oxidation.

2. Experimental

2.1. Materials preparation

The mixed copper (II) acetate and manganese (II) acetate were prepared by physical grinding of the two salts (Sigma Aldrich 98% ACS reagent) and by supercritical anti-solvent (SAS) precipitation. For both processes a conventional molar ratio of 2:1 Mn:Cu was used. Physically mixed samples were ground together in a pestle and mortar for 10 min before being pelleted. The material was then ground again, re-pelleted and ground again. The SAS precipitated material was prepared using an apparatus described elsewhere [7]. Materials were prepared using a solution of the acetate salts (Sigma Aldrich 98% ACS reagent) with DMSO (99.9% ACS reagent) as the solvent. The solution was then sprayed into supercritical CO_2 at 110 bar and 40 °C. The CO_2 acts as an anti-solvent by diffusing into the DMSO solution, making the acetate salts supersaturated in the now expanded solution. The subsequent precipitate was dried for 30 min in a stream of flowing supercritical CO_2 under the same conditions used for the preparation.

2.2. Characterisation and in situ studies

Thermogravimetric analysis (TGA) was performed using a Setaram Labsys in conjunction with differential temperature analysis (DTA). 10–30 mg of the sample was loaded into alumina crucibles, heated to 400 °C (at 1, 5 and 10 °C min^{-1}) in a synthetic air/N_2 atmosphere and held for 10 min before cooling. For each ramp rate a blank run was carried out and the results were subtracted from the relevant data, to remove buoyancy effects.

Investigation of the bulk decomposition of copper and copper/manganese acetate was carried out using an X'pert Pro XRD fitted with an Anton-Parr XRK900 *in situ* cell (internal volume of ~0.5 L). The sample mass used was dictated by the sample holder volume and was ~0.15 g. Experiments were carried out under various atmospheres: pure He, 10 vol% O_2 in He, 20 vol% O_2 in He and static air, with flows of 0, 15 and 30 ml min^{-1}. The heating rate was 10 °C min^{-1} with diffraction patterns collected every 10 °C. For the copper only materials each data collection scan was between 35° and 45° 2θ where reflections from the acetate, CuO, Cu_2O and Cu could be detected, while the range was extended from 25° to 45° 2θ for mixed metal salt systems. The final temperatures after heating varied between 350 and 400 °C.

High resolution transmission electron microscopy (HRTEM) was carried out using a Jeol 3010 transmission electron microscope operated at 300 kV. Fast Fourier transform has been used to obtain diffraction patterns. In addition scanning transmission electron microscopy (STEM) was used to map elemental distribution of copper and manganese. Temperature programmed reduction was performed using a Thermo TPDRO 1100 series to gain information on the reduction potential of the heat-treated samples. X-ray photoelectron spectroscopy measurements were made using a Kratos Axis Ultra DLD spectrometer using monochromatised Al Kα radiation, and analyser pass energies of 160 eV (survey scans) or 40 eV (detailed scans). Binding energies are referenced to the C (1s) peak from adventitious carbonaceous contamination, assumed to have a binding energy of 284.7 eV.

2.3. Catalyst testing

Materials tested for CO oxidation were heat treated at 300 °C under flowing air, static air and flowing helium. A lower heat treatment temperature than that used for the *in situ* XRD analysis was employed in order to limit the degree of crystallinity, as highly ordered material has been shown to be detrimental to the catalyst performance [17]. The activity was determined by passing 5000 ppm CO in synthetic air, at a flow rate of 22.5 ml min^{-1} through 50 mg of the catalyst that was held in a quartz tube. The sample temperature was maintained at 25 °C using a thermostatically controlled water bath. CO conversion was determined by on-line gas chromatography using a Varian 3800 GC.

3. Results

3.1. Copper acetate thermal decomposition

The TGA/DTA profiles of the of $Cu(ac)_2{\cdot}H_2O$ samples heat treated in air and nitrogen at 10 °C min^{-1} are shown in Fig. 1a and b.

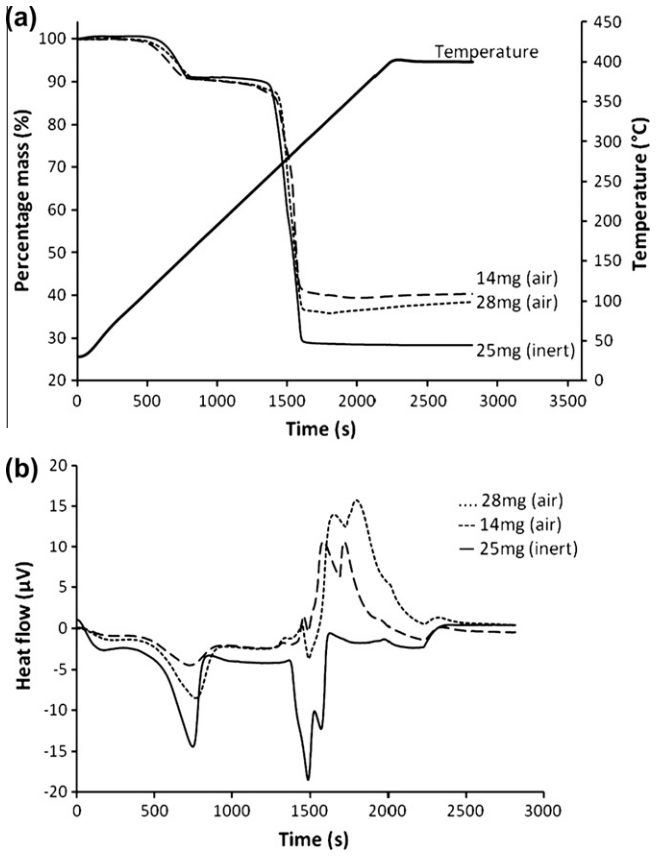

Fig. 1. TGA and DTA of copper acetate under inert conditions and air: (a) TGA, (b) DTA.

It was noted that under flowing air the mass loss varied considerably depending on the initial mass (Table 1). Calculated theoretical mass losses for copper acetate monohydrate decomposition (Table 1) showed that the maximum mass loss of the two samples correlated with CuO for the smaller sample and Cu_2O for the larger. Water loss occurred in the region of 150–175 °C as indicated by the mass loss and the endotherm in the DTA. The decomposition of the acetate then continues through a single mass loss starting at 250 °C. However, several distinct exotherms were apparent between 250 and 350 °C. It was noted that samples under air flow had a mass gain occurring after the decomposition of the acetate, which would indicate the oxidation of Cu^+ or Cu and the significant exotherms around 320 °C would agree with this assignment. For larger samples the mass gain was around 2.7%, whilst using smaller samples the gain was only 1%. This indicates a significant oxidation of predominantly Cu^+ to Cu^{2+} in the larger sample, whilst the smaller sample was re-oxidised to a lesser extent. This is in agreement with the total mass losses, which show that the smaller sample with the lower mass gave minimal reduction, whilst it indicated total Cu^+ formation in the larger mass sample. This variable degree of reduction is in agreement with the literature and provides a note of warning that the effects of heat treatment are significantly affected by sample mass and flowing gas composition [13].

Table 1
Effect of sample mass on observed TGA mass losses.

Sample	Sample mass (mg)	Mass loss from H_2O (%)	Mass loss from acetate (%)	Total mass loss (%)	Weight gain (%)
Nitrogen (a)	25	9.0	62.7	71.8	0.0
Air (a)	14	9.4	50.2	59.6	1.0
Air (b)	28	9.7	54.7	64.4	2.7

The mass losses from copper acetate monohydrate to give: CuO = 60.1%, Cu_2O = 64.2%, Cu = 68.2%.

Studies using a N_2 atmosphere showed total decomposition to copper metal over the same temperature range as the decomposition in air. Total decomposition was confirmed by lack of mass gain above 300 °C, which was observed for the TGA experiment in air. The main exotherms seen under air were not present and were replaced by an endotherm at a slightly lower temperature, as observed in the literature [8].

3.2. In situ XRD of the decomposition of $Cu(CH_3COO)_2{\cdot}H_2O$

Fig. 2a–c shows the diffraction patterns for decomposition under static air. The crystalline acetate phase disappears between 110 °C and 140 °C to leave a predominantly amorphous phase (broad peak observed at 38.1° 2θ). This is in agreement with the TGA analysis and is attributed to the loss of coordinated H_2O to form dehydrated copper acetate.

The next observable phase change occurred at 240 °C with broad peaks matching the reflections of CuO becoming apparent at 35.7° and 38.7° 2θ (scans at 240–260 °C expanded for clarification of CuO formation in supplementary). At 250 °C a pattern associated with Cu_2O was observed, which increased in intensity with increasing temperature up to 280 °C. During this time the reflections associated with CuO diminished and were no longer observable after 270 °C. At 290 °C a reflection assigned to copper metal at 43.3° 2θ is observed, which increased in intensity with further heating, whilst the Cu_2O diffraction intensity decreased.

Several of the phase changes observed during the *in situ* XRD experiment are in agreement with the TGA data. The initial phase change between 110 and 140 °C coincides with the endothermic mass loss associated with the dehydration of the coordinated water. The next stage of mass loss was recorded between 200 and 300 °C, with a gradual loss occurring up to 250 °C which then accelerates significantly. This corresponds to the onset of oxide formation and the reduction to copper metal. The difference between XRD and TGA of the decomposition of samples in air was that the XRD showed total reduction to copper metal and no re-oxidation, while the TGA showed incomplete reduction (based on the maximum observed mass loss) and re-oxidation of the material that had reduced. This was attributed to the flowing conditions of the TGA experiments facilitating re-oxidation and the removal of the reducing products formed during the decomposition. An additional implication is that all the oxygen present was consumed in the static air experiment (cell volume ~0.5 L).

A comparison of the decomposition of copper acetate under different atmospheres is shown in Fig. 3, helium, 10% oxygen in helium and 20% oxygen in helium were investigated and the counts of the most intense reflection associated with the different phases (CuO – 35.7° 2θ, Cu_2O – 36.7° 2θ, Cu – 43.3° 2θ) were plotted against temperature.

It was noted that for all conditions the formation of copper oxide phases started at 230 °C. In all experiments the trend of $Cu^{2+} \rightarrow Cu^+ \rightarrow Cu$ was observed with the temperature of formation of CuO and Cu_2O being comparable in all experiments. The temperature of formation of copper metal differed between the 10% and 20% oxygen containing atmosphere, with the former yielding Cu at ~350 °C and the latter at 280 °C. The onset of Cu formation in the flowing 20% oxygen sample was comparable with the static air experiment. As shown previously acetate decomposition is endothermic in an inert atmosphere and exothermic in air. It is envisaged that the exothermic reaction in the 20% oxygen containing atmosphere provided additional heat that significantly

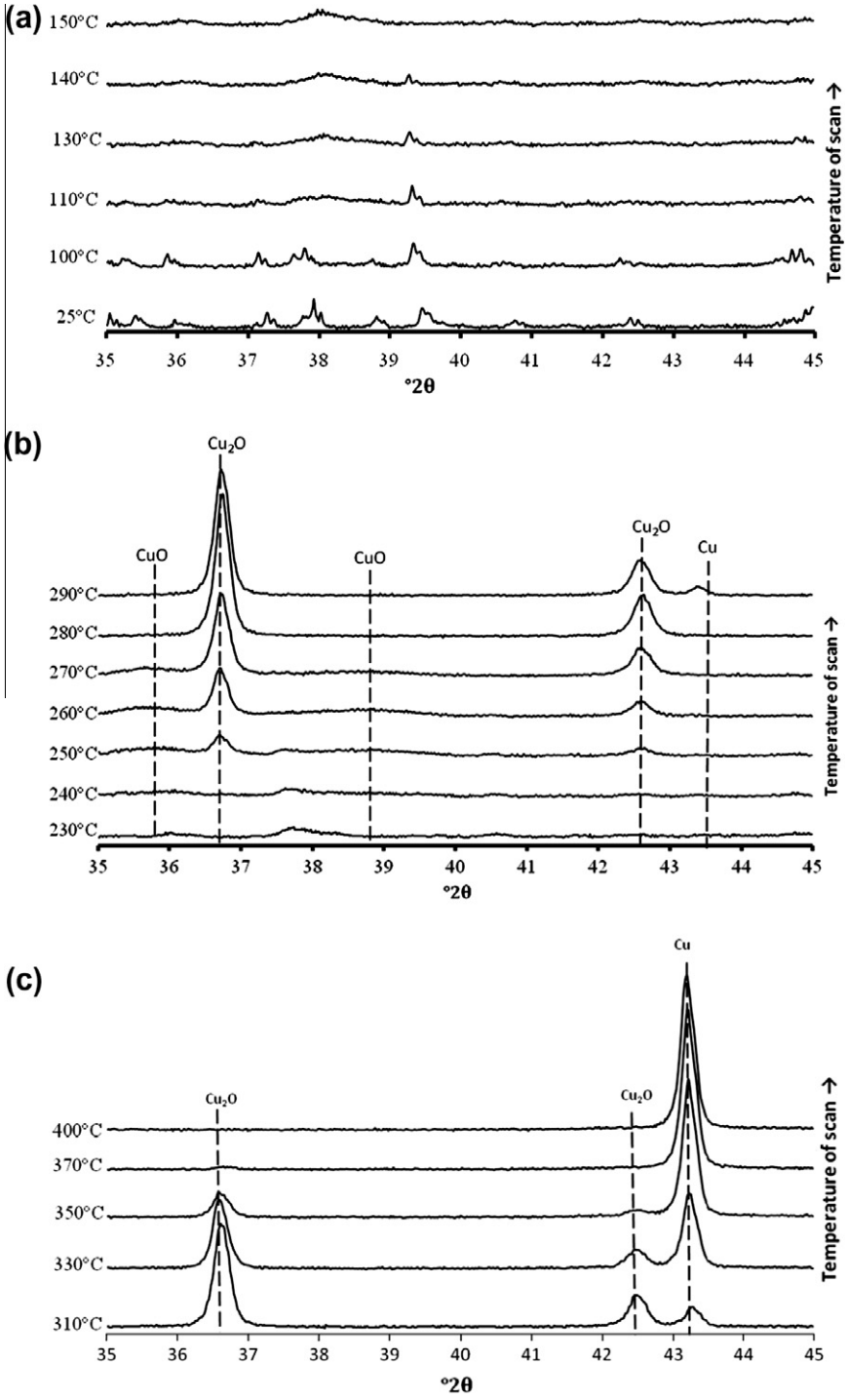

Fig. 2. *In situ* XRD of copper acetate decomposition under static air: (a) dehydration of copper acetate monohydrate 25–140 °C, (b) copper oxide reduction 230–290 °C, (c) full metallic copper formation 310–390 °C.

increased the rate of decomposition. It was observed that re-oxidation of the samples occurred in the presence of flowing oxygen, with the concentration of oxygen significantly affecting the degree of oxidation.

The transient reduction to copper metal under all atmospheric conditions has not been observed previously and demonstrates the powerful reduction potential of the evolved gas during the acetate decomposition. In addition, the final oxidation state of the copper has been shown to be easily controlled by adjustment of the oxygen content.

A further set of studies were performed, which investigated the effect of increased gas flow rates (30 ml min^{-1} helium) during decomposition. It was observed that under all conditions the CuO and Cu_2O phase changes occurred at the same temperatures. This resulted in the formation of Cu under all conditions except 20% oxygen in helium. The difference observed under this atmosphere was considered to be due to the rapid re-oxidation of the metal phase under these oxidising conditions. The rate of phase change was noticeably faster at higher flow rates. Fig. 4 shows the relative changes in copper phases by plotting the counts of the most

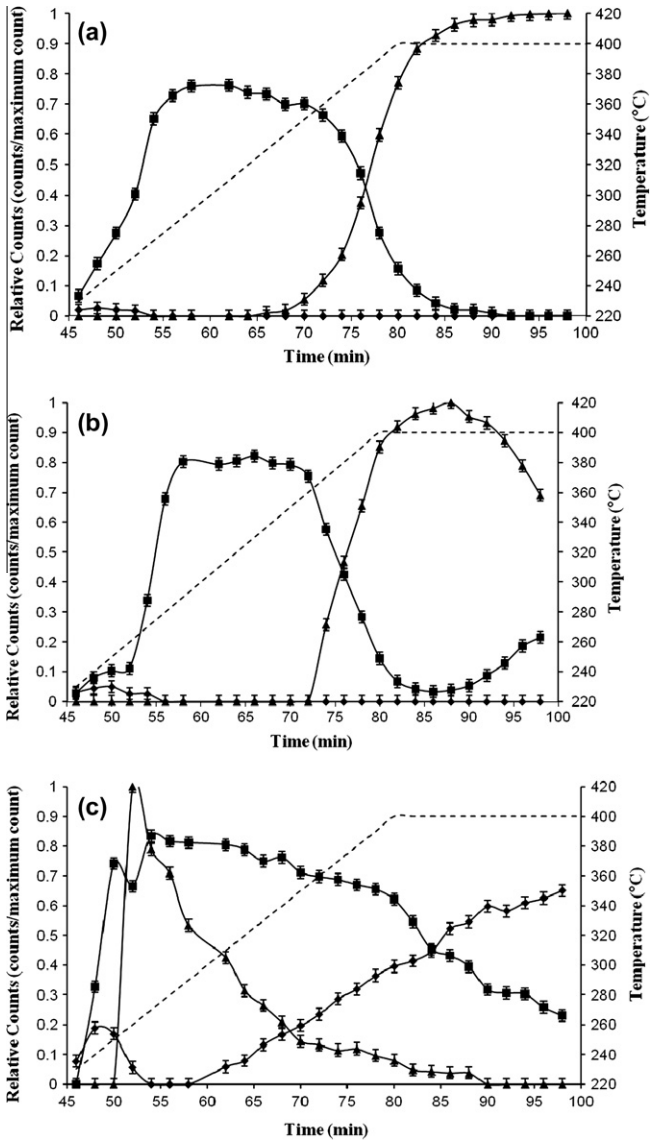

Fig. 3. Plot of counts from principal copper phase reflections of *in situ* XRD analysis of copper acetate decomposition under various conditions: (a) helium flow, (b) 10% oxygen atmosphere, (c) 20% oxygen atmosphere. Phases: (▲) Cu, (■) Cu_2O, (●) CuO.

intense reflection for each phase as the temperature is increased. These data were considered to be in agreement with previous studies [13], which related the retention time of inhibiting gases over the acetate salt to the decomposition rate. The formation of acetic acid is considered to inhibit decomposition with lower retention times of the compound subsequently increasing the rate.

3.3. Thermal decomposition of physically mixed copper and manganese acetates

XRD analysis of the physically mixed copper (II) acetate and manganese (II) acetate (Fig. 5) was used to determine the final phases after heat treatment at 350 °C in flowing air and inert helium for 2 h. Under oxygen-rich conditions the mixed acetates formed Hopcalite (ICDD 01-075-0826), along with copper oxide (CuO, ICDD 01-070-6831) and manganese oxide (Mn_3O_4, ICDD 00-008-0017). The formation of separate metal oxide species in the physically mixed sample is due to the relatively poor degree of mixing between acetate salts.

In situ XRD of the physically mixed material heat treated under oxygen-rich conditions (Fig. 6) shows the presence of Cu_2O phases at 250 °C with Mn_3O_4 reflections observable from 260 °C. Both sets of reflections for the phases remained relatively constant until 360 °C when Cu_2O reflections began diminishing, and CuO reflections were simultaneously observed. No Cu metal reflections were observed throughout the analysis, which were observed in the analogous copper acetate decomposition. This implies that autoreduction of the copper complex has been partially limited by the presence of a manganese phase. In addition, no mixed phase spinel structure was observed during the *in situ* experiments. The formation of crystalline Hopcalite is thought to come from the interaction between the stable re-oxidised CuO phase and Mn_3O_4, with Hopcalite formation occurring due to the metal ion migration at the Cu/Mn oxide phase boundaries to form the spinel structure.

Under an inert atmosphere, a mixture of copper metal (ICDD 03-065-9743) and manganese (II) oxide (ICDD 01-075-0625) is formed (Fig. 5). It is clear that, not only has each of the component metal compounds been reduced, but that formation of an ordered Hopcalite spinel has been totally inhibited. *In situ* XRD analysis of the material under helium flow (Fig. 7) shows the formation of Cu_2O at 240 °C which increases in intensity until 340 °C. At this temperature, reflections associated with Mn_3O_4 became apparent and remained observable until 380 °C. The Mn_3O_4 reflections began to diminish at 350 °C with the formation of MnO and Cu metal phases starting at 320 °C. These phases then increase with the Cu_2O and Mn_3O_4 phases diminishing. Comparison between the evolution of copper phases between the copper/manganese acetate sample and the copper only sample is similar to Cu_2O and Cu reflections being observed at comparable temperatures. The extinction of the copper oxide phase was slower in the mixed sample, and with the presence of Mn_3O_4, indicating retardation of the reduction of the copper phases.

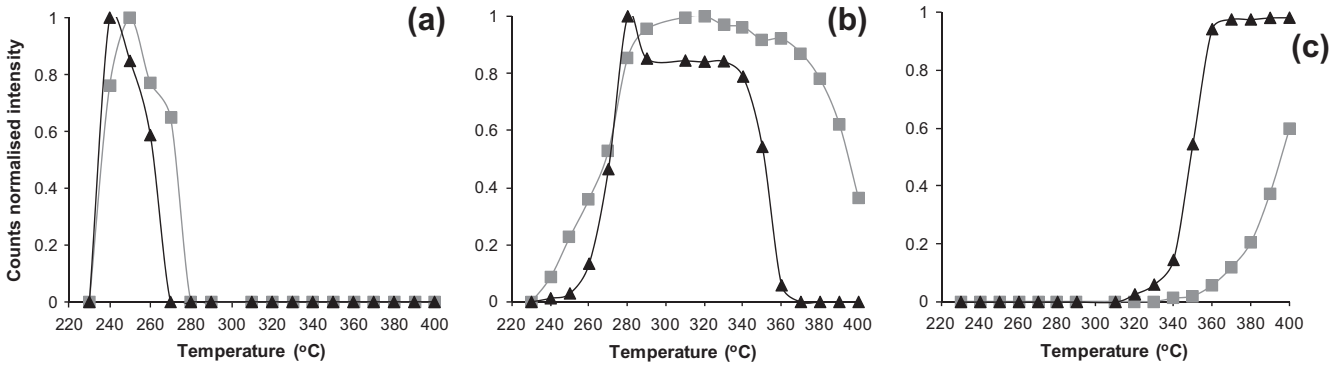

Fig. 4. Plot of principal copper reflections of *in situ* XRD analysis of copper acetate decomposition with variable flow rates under helium atmosphere. (a) CuO formation, (b) Cu_2O formation, (c) Cu formation. (▲) 30 ml min^{-1}, (■) 15 ml min^{-1} flow rates.

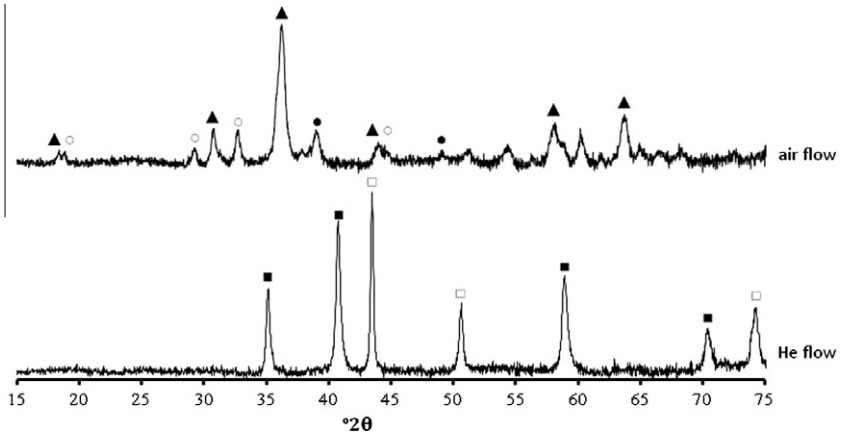

Fig. 5. XRD of a physical mixture of copper/manganese acetate heat treated under helium and 20% oxygen atmosphere. Phase assignment: (▲) $CuMn_2O_4$, (◇) Cu_2O, (■) MnO, (○) Mn_3O_4, (□) Cu, (●) CuO.

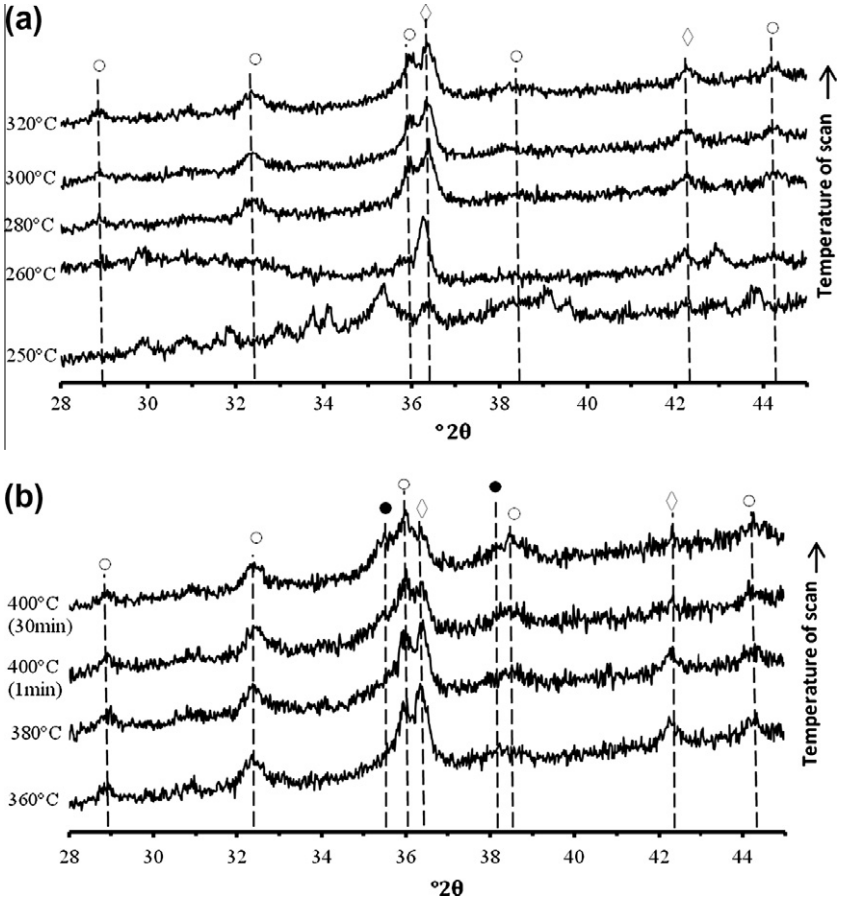

Fig. 6. *In situ* XRD of copper/manganese acetate decomposition under flowing air: (a) 250–320 °C, (b) 320–400 °C. (○) Mn_3O_4, (◇) Cu_2O, (●) CuO.

3.4. Thermal decomposition of supercritically precipitated copper and manganese acetates

Following the investigation of the commercial copper and copper/manganese acetates and the observation of auto-reduction inhibiting spinel formation, the effect of the degree of mixing between metal salts was investigated. The high degree of mixing facilitated by SAS precipitation in supercritical media allows for intimately mixed copper (II) and manganese (II) acetates [7].

The heat treatment of the SAS prepared copper and manganese acetate precursor showed a similar trend to the physically mixed samples. The sample that was heat treated under flowing air produced a sample that was characterised as Hopcalite by XRD (Fig. 8). The principal differences between the SAS prepared sample and the physically mixed acetates (Fig. 5) were the change in Hopcalite crystallite size and the presence of copper and manganese oxide phases in the physically mixed material. The Hopcalite crystallites sizes, determined from the (3 1 1) plane, were *ca.* 6 nm and 14 nm, for the SAS and physically mixed samples, respectively. The reduction in crystallite size, due to SAS precipitation, can be attributed to the small and well-mixed acetate particles formed because of rapid nucleation facilitated by the SAS process. The lack of

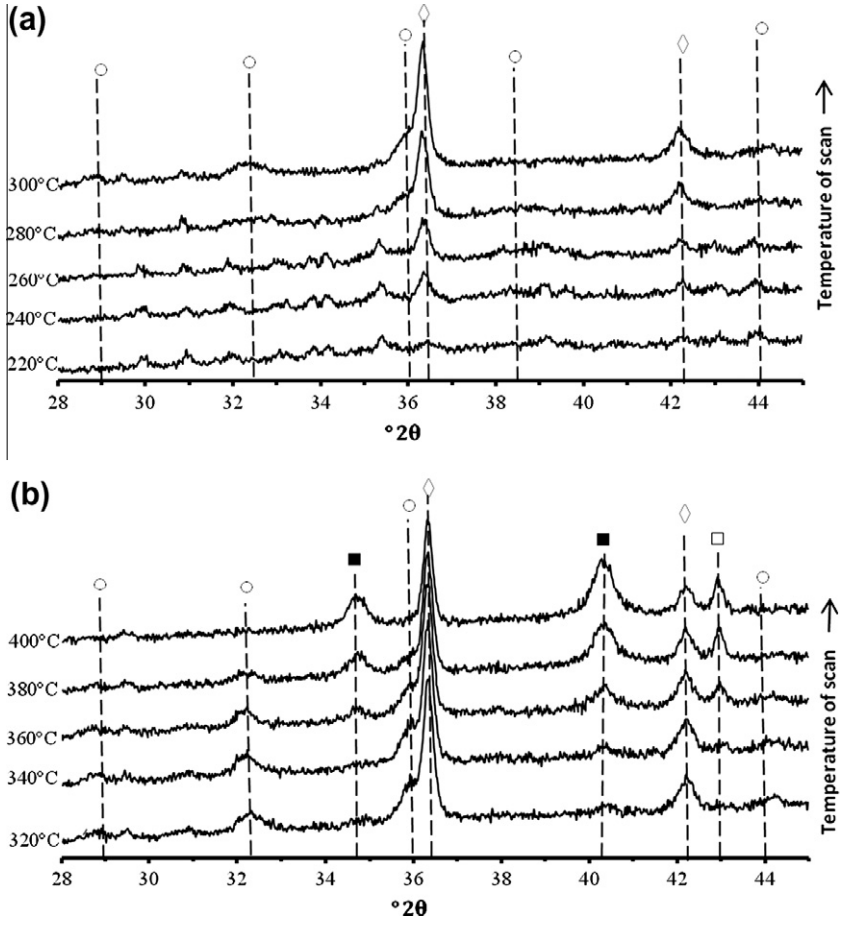

Fig. 7. *In situ* XRD of copper/manganese acetate decomposition under flowing helium: (a) 220–300 °C, (b) 320–400 °C. (○) Mn_3O_4, (■) MnO, (◇) Cu_2O, (□) Cu.

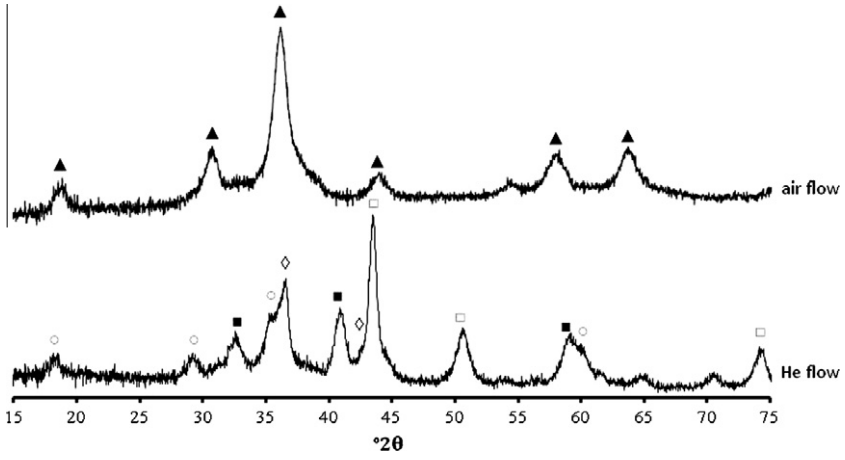

Fig. 8. XRD of mixture of copper/manganese acetate from SAS precipitation under helium and 20% oxygen atmosphere. Phase assignment: (▲) $CuMn_2O_4$, (◇) Cu_2O, (■) MnO, (○) Mn_3O_4, (□) Cu.

discrete metal oxides in SAS precipitated materials can also be attributed to the significantly improved mixing of the metal acetates in the SAS prepared sample, facilitating metal ion restructuring and consequently Hopcalite formation.

Under an inert atmosphere the heat-treated SAS prepared material comprised of metallic copper and Cu_2O. The crystallite size of the metallic copper was determined to be *ca.* 14 nm using the Scherrer equation. Manganese containing phases, Mn_3O_4 and MnO, were also observed for the SAS precipitated material, whereas Cu_2O and Mn_3O_4 phases were not observed in the final physically mixed sample. This intermediate mixing of metal oxides can be seen by HRTEM (Fig. 9), which shows highly mixed Cu_2O and Mn_3O_4 phases. The presence of higher oxidation state phases could be the result of a greater degree of surface interaction between the easily oxidisable manganese phase and the highly reducible copper phase. As the copper phase auto-reduces, the

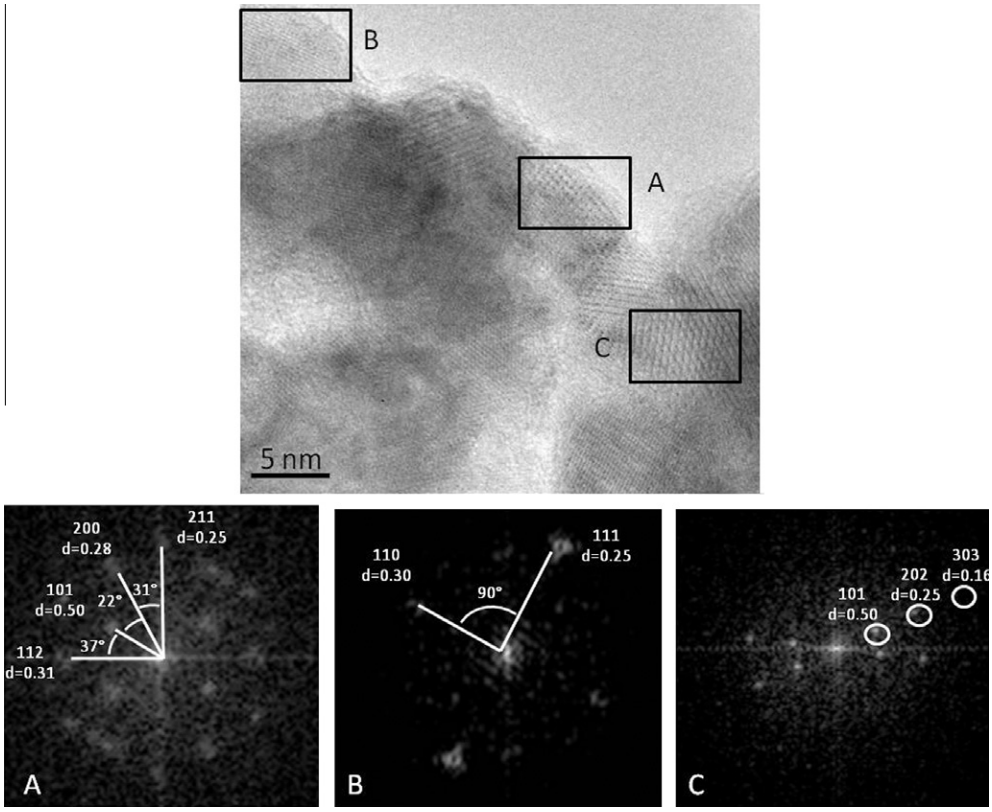

Fig. 9. HRTEM image of SAS prepared copper/manganese acetate heat treated under helium. Marked regions and FFTs show; Mn_3O_4 (space group I41) in regions A and C, Cu_2O (space group pn-3m) in region B.

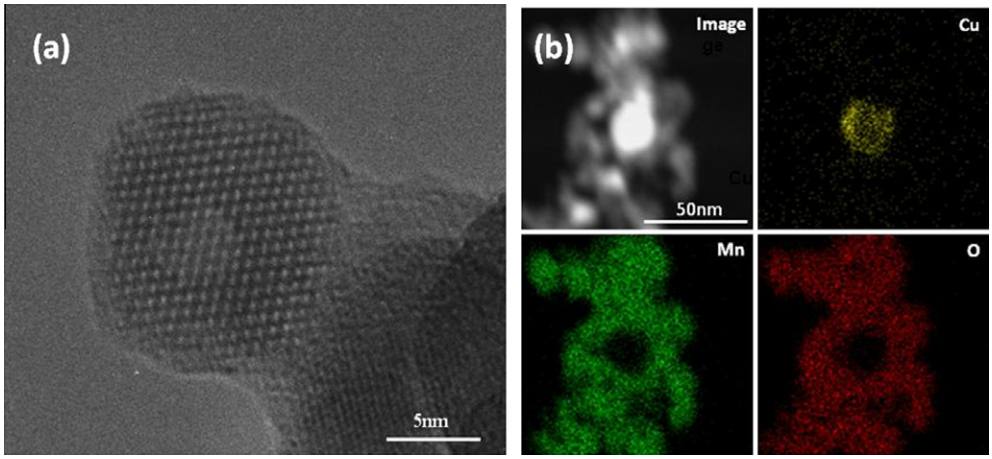

Fig. 10. HRTEM and STEM analysis of copper particles formed by heat treatment under helium. (a) HRTEM image, (b) image and EDS elemental maps from STEM.

oxygen liberated from the acetate ligand can be retained by the manganese phase. This oxidised manganese phase can then donate oxygen back to the copper phase and effectively retard copper reduction. Alternatively, manganese oxide phases could oxidise CO formed from acetate decomposition and so limit the potential for reduction. The presence of the $Mn^{2+/3+}$ oxidation states in the Mn_3O_4 phase is clear evidence of partial oxidation, from the original Mn^{2+} present in the acetate complex, within a predominantly reducing system. The presence of a Mn^{3+} containing phase is not seen in the decomposition of manganese (II) acetate under a helium atmosphere (supplementary data), and so its presence in the copper/manganese sample supports the idea of oxygen being transferred from the copper species.

The presence of the manganese phase has been shown to stabilise smaller copper metal crystallites. Unsupported copper metal formed by auto reduction at 350 °C in flowing helium at 15 ml min^{-1} had a crystallite size of *ca.* 46 nm, while the mixed phase produced from SAS precipitation, under the same conditions, had a copper crystallite size of *ca.* 14 nm. The presence of these small copper crystallites is confirmed by HRTEM and STEM (Fig. 10) analysis of the copper/manganese material formed by the heat treatment under inert conditions. EDS mapping in the STEM clearly shows the phase separation of the Cu and the manganese oxide (Fig. 10b). This reduction in crystallite size can be attributed to the manganese oxide acting as a simple spacer between copper crystallites and subsequently preventing sintering

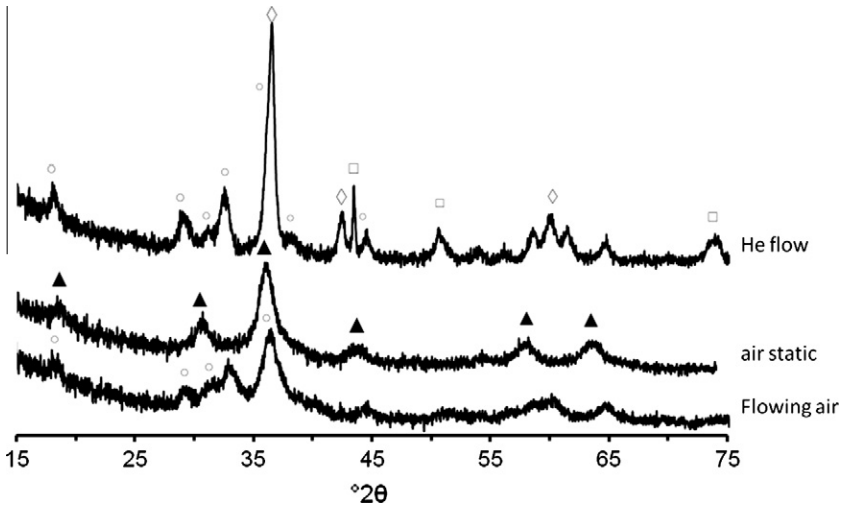

Fig. 11. XRD of mixture of copper/manganese acetate from SAS precipitation 300 °C heat treatment. Phase assignment: (▲) $CuMn_2O_4$, (◇) Cu_2O, (■) MnO, (○) Mn_3O_4, (□) Cu.

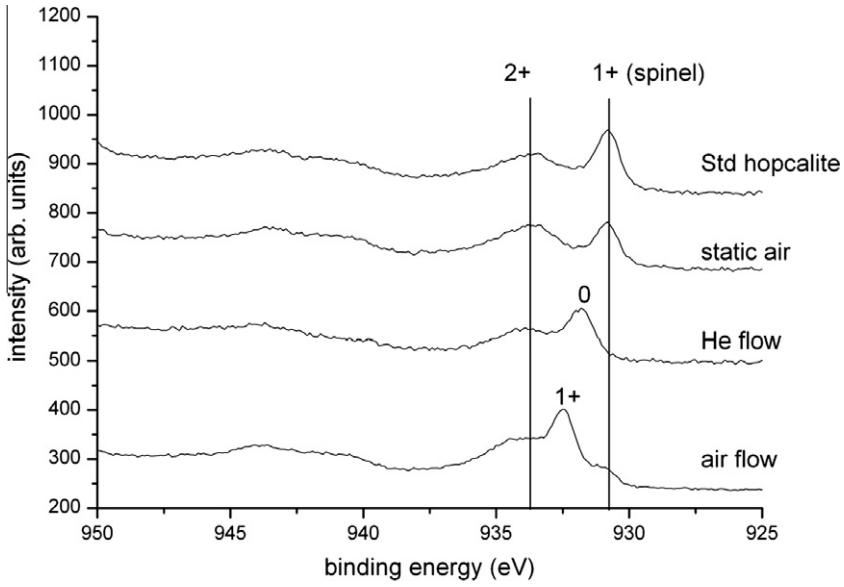

Fig. 12. Cu 2p XPS of copper/manganese acetate heat treated in different atmospheres. Numbers indicate assigned copper oxidation state.

during heat treatment. In addition, the interaction between the copper and manganese phases during decomposition facilitates the formation of stable metal oxide interfaces.

3.5. Carbon monoxide oxidation of heat treated mixed acetates

Materials tested for CO oxidation were heat treated at 300 °C under both flowing air and helium. The observations made from the studies of copper acetate, with respect to the influence of flow rate have shown that the parameter can be influential on the composition of phases in the activated material. Subsequently heat treatment was also carried out under static air. A lower heat treatment temperature than that used for the *in situ* XRD analysis was used in order to limit the degree of Hopcalite crystallinity, as highly ordered material has been shown to be detrimental to the activity [17].

The trend observed during the *in situ* studies was consistent with XRD analysis of the 300 °C heat-treated samples (Fig. 11). Materials formed in oxygen-rich environments gave Hopcalite along with Mn_3O_4, whilst under inert conditions reduced copper phases were formed. The degree of reduction in the sample treated under helium was less than that obtained at higher temperature during the *in situ* XRD experiments. The major phases observed were Cu_2O and Mn_3O_4 with a small amount of copper metal. Some copper metal can be formed at 300 °C, but total reduction is facilitated by higher temperatures. Heat treatment under flowing air resulted in a material with crystalline manganese oxide phases and no observable copper phases, and hence differed from the Hopcalite formed at a higher temperature. Calcination in static air resulted in the Hopcalite phase formation. From the *in situ* studies of copper acetate decomposition it was observed that the static conditions facilitated a greater auto reduction than the flowing conditions, with slower oxidation of Cu and Cu_2O. It is apparent that slowing the rate of phase change has allowed for ion migration and the formation of the Hopcalite phase at a lower temperature.

The Cu 2p XPS of the phases is shown in Fig. 12. A spectrum of a standard Hopcalite has been used for comparison, with Cu binding energies of the standard Hopcalite being indicative of Cu^{2+} and Cu^{+}.

The Cu^{+} binding energy in the Hopcalite structure lies at a lower energy than the Cu metal due to its position in the octahedral sites in the spinel structure [18]. In agreement with XRD the spectra for the static air sample comprised of Cu^{2+} and Cu^{+} at binding energies associated with the standard Hopcalite.

Calcination under flowing air resulted in the Cu^{2+} and Cu^{+} signals in addition to a dominant signal at 932.5 eV, assigned as Cu^{+} not incorporated into the spinel structure. The presence of Cu^{2+} and Cu^{+} binding energies associated with Hopcalite shows that the phase is beginning to form under the flowing air conditions. The Cu^{+} present is considered to be a precursor phase to Hopcalite, where Cu ions are migrating into the Mn_3O_4 lattice.

Heat treatment under inert helium resulted in no Cu^{+} signal associated with incorporation of copper into a spinel structure, with the predominant signal assigned as Cu^{0} dispersed by manganese oxide. This is in agreement with the XRD of the specific sample and *in situ* studies. While Cu_2O is present within the bulk of the sample according to XRD, its presence on the surface is not apparent due to overlap from signals at 931.9 eV and 934.3 eV. The presence of Cu^{2+} on the surface illustrates the ability of manganese phases to stabilise copper oxidation states at the Cu/Mn interface.

The Mn 2p XPS is not frequently investigated for Hopcalite samples, due to the difficulties in deconvolution of Mn^{3+} and Mn^{4+} [18]. This was the case for the materials produced under oxygen containing atmospheres (spectra given in supplementary). However, the spectra of the sample produced under helium atmosphere showed predominantly Mn^{2+} with a small signal associated with Mn^{3+}, in agreement with observations of MnO and some Mn_3O_4 from XRD analysis.

The materials heat treated in static air, flowing air and helium were tested as catalysts for ambient temperature CO oxidation (Fig. 13). The presence of low binding energy Cu^{+}, associated with Hopcalite, directly correlates with the sample's catalytic activity. The inactive sample produced under helium flow was the only sample not to have any evidence of a Hopcalite spinel phase. The most active sample comprised of bulk Hopcalite with no other phases being seen. The less-active sample, although having some spinel structure according to XPS, was predominantly formed of crystalline Mn_3O_4 and an amorphous Cu^{+} phase.

The importance of the spinel structure resulting in activity illustrates the requirement of electronic transfer between copper and manganese to provide a redox mechanism [19], as shown in Eq. (5)

$$Cu^{2+}Mn^{3+} \leftrightarrow Cu^{1+}Mn^{4+} \quad (5)$$

The inactivity of phase-separated Cu and Mn oxides shows that the current study finds no support for a spill-over mechanism that has been proposed previously [6], which suggests that CO adsorbs, and is oxidised by CuO which is itself re-oxidised by an oxygen donating Mn^{3+} oxide. The formation of the spinel phase is considered to inhibit this mechanism, while the current work shows that a spinel phase is required for the activity. In addition the phase-separated copper and manganese oxides produced by treatment under inert conditions, considered favourable for spill-over reactions due to the presence of surface Cu^{2+} and Mn^{3+}, proved to be inactive.

Recent TAP experiments to elucidate the mechanism of Hopcalite and Au-doped Hopcalite have shown that both Mars van Krevelen and Langmuir–Hinshelwood mechanisms are observed in active materials [20]. It was demonstrated that the Mars van Krevelen mechanism was predominant with Au enhancing the mechanism by facilitating the reducibility of the Hopcalite. XPS analysis of the Au-doped materials showed the enhancement of Cu^{+}, with a similar binding energy to the active phase determined in the current study. It was demonstrated that incorporation of Au increases reducibility, which promotes Mars van Krevelen

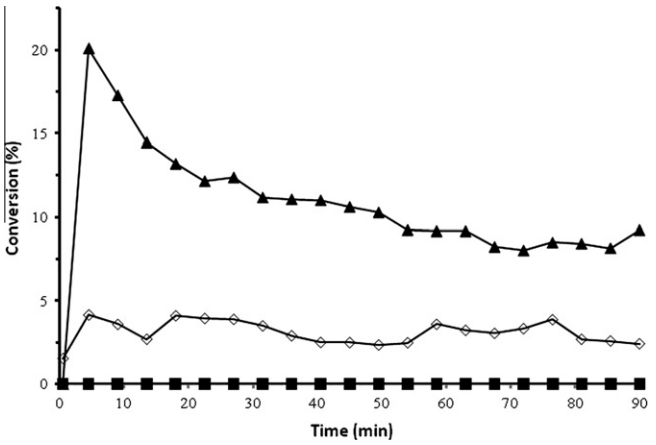

Fig. 13. Conversion of CO at 25 °C over the copper/manganese acetate heat treated in different atmospheres (5000 ppm CO, 50 mg of catalyst, GHSV 12,000 h^{-1}). (▲) Static air, (◇) flowing air, (■) flowing helium.

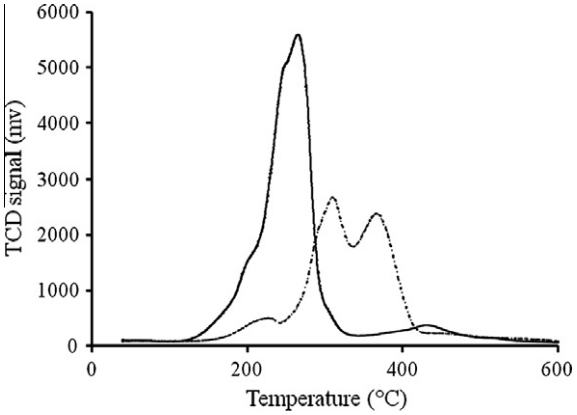

Fig. 14. Temperature program reduction of SAS copper/manganese acetates heat treated under different atmospheres. (—) Static air, (- - -) helium.

reactions and increases activity. Although the current study does not explore the mechanism of CO oxidation it does support the proposal that catalysts with greater redox potential are active for CO oxidation [21].

In addition to the correlation between XPS findings in this study and the previous Au-doped study, TPR analysis highlights the change in the reduction potential of different catalysts produced by heat treatment of the metal acetates. A detailed interpretation of Hopcalite TPR profiles is inherently difficult, due to the multiple possible valencies of both copper and manganese oxides. However, the clear change in the temperature of reduction (Fig. 14) between the active catalysts calcined in static air and the inactive materials heat treated in helium is in agreement with the Au doping study [21]. The predominant reduction temperature for the active material *ca.* 260 °C is significantly lower than the two principal reduction peaks at *ca.* 305 and 360 °C. This simply illustrates that the ease of reducibility correlates with the activity of the material.

4. Conclusions

The current investigation of the decomposition of copper acetate using *in situ* XRD techniques in combination with XPS and electron microscopy has confirmed and further clarified aspects of the mechanism of CO oxidation. Phase changes show the reduction of the Cu^{2+} salt to copper metal under a limited supply of oxygen. The effect of oxygen was shown to be significant in terms

of both concentration and flow rate, with 20% oxygen content resulting in a lower reduction temperature. Under a static O_2-containing atmosphere the resulting copper metal did not oxidise, unlike the samples heat treated under flowing oxygen. Limited oxygen supply (10% O_2) resulted in a decomposition that was similar to that observed under inert helium, but with a slower rate of oxidation. It can be concluded that the oxidation state of copper can be tailored by altering both the oxygen content of the atmosphere and the heat treatment time.

The presence of manganese acetate with copper acetate results in a range of phases being formed under heat treatment and the phases formed were dependent on the oxygen content and the degree of surface interaction between the two acetate salts. Materials heat treated under an oxygen-containing atmosphere formed the Hopcalite spinel phase, while oxygen-free atmospheres resulted in the reduction of copper phases to produce copper metal and manganese oxide phases. Samples prepared using a SAS precipitation technique showed a greater degree of interaction between the two metal salts, with a single Hopcalite phase being formed under oxygen-rich atmospheres and evidence of the retardation of copper oxide reduction by manganese phases under oxygen-deficient conditions, to give residual Cu_2O and $Mn^{2+/3+}$ oxide phases. The reduction of the heat treatment temperature to 300 °C resulted in the formation of materials similar to those produced at 350 °C. However, there was less reduction under inert atmospheres and limited Hopcalite spinel formation under oxygen-containing atmospheres. XPS showed that Cu^{2+} and Cu^{+} were present on all surfaces, but that spinel formation was present in oxygen heat-treated samples only.

The ability to control phase formation allows investigation into their catalytic potential for CO oxidation. Activity can be correlated with the presence of the $CuMn_2O_4$ spinel, with higher content resulting in higher activity. This strongly supports the spinel redox mechanism, while showing no evidence for a spill-over mechanism. Although it has been shown that heat treatment under inert conditions produces inactive CO oxidation catalysts, the process demonstrates the potential for a single simple step protocol to form supported metal nano-particles on a metal oxide support without hydrogen reduction. The total inhibition of the Hopcalite mixed metal oxide under these conditions illustrates that discrete phases can be maintained, which could be applicable for other catalytic reactions.

Acknowledgments

We wish to thank Johnson Matthey, the EPSRC and CIKTN for the provision of a case award to S.A.K.

Appendix A. Supplementary data

Supplementary data associated with this article can be found, in the online version, at doi:10.1016/j.jcat.2011.05.012.

References

[1] A.A. Mirzaei, H.R. Shaterian, M. Kaykhaii, Appl. Surf. Sci. 239 (2005) 246.
[2] Y. Tanaka, T. Takeguchi, R. Kikuchi, K. Eguchi, Appl. Catal. A 279 (2005) 59.
[3] H. Chen, X.L. Tong, Y.D. Li, Appl. Catal. A 370 (2009) 59.
[4] S.K. Agarwal, J.J. Spivey, J.B. Butt, Appl. Catal. A 81 (1992) 239.
[5] G.J. Hutchings, A.A. Mirzaei, R.W. Joyner, M.R.H. Siddiqui, S.H. Taylor, Appl. Catal. A 166 (1998) 143.
[6] F.C. Buciuman, F. Patcas, T. Hahn, Chem. Eng. Process. 38 (1999) 563.
[7] Z.R. Tang, C.D. Jones, J.K.W. Aldridge, T.E. Davies, J.K. Bartley, A.F. Carley, S.H. Taylor, M. Allix, C. Dickinson, M.J. Rosseinsky, J.B. Claridge, Z.L. Xu, M.J. Crudace, G.J. Hutchings, Chemcatchem 1 (2009) 247.
[8] M.D. Judd, B.A. Plunkett, M.I. Pope, J. Therm. Anal. 6 (1974) 555.
[9] A.Y. Obaid, A.O. Alyoubi, A.A. Samarkandy, J. Therm. Anal. Calorim. 64 (2000) 985.
[10] J.C. De Jesus, I. González, A. Quevedo, T. Puerta, J. Mol. Catal. A 228 (2005) 283.
[11] T. Wanjun, C. Donghua, Chem. Paper 61 (2007) 329.
[12] S.V. Pol, V.G. Pol, I. Felner, A. Gedanken, J. Inorg. Chem. 14 (2007) 2089.
[13] J. Leicester, M.J. Redman, J. Appl. Chem. 12 (1962) 357.
[14] Y. Lin, K.A. Watson, M.J. Fallbach, S. Ghose, J.G. Smith, D.M. Delozier, W. Cao, R.E. Crooks, J.W. Connell, ACS Nano 3 (2009) 871.
[15] J.C. De Jesus, J. Vac. Sci. Technol. A 26 (2008) 913.
[16] J.B. Gadhe, Int. J. Hydrogen Energy 32 (2007) 2374.
[17] C.D. Jones, K.J. Cole, S.T. Taylor, M.J. Crudace, G.J. Hutchings, J. Mol. Catal. A 305 (2009) 121.
[18] S. Veprek, D.L. Cocke, S. Kehl, H.R. Oswald, J. Catal. 100 (1986) 250.
[19] G.M. Schwab, S.B. Kanungo, Z. Phys. Chem. Neue Fol. 107 (1977) 109.
[20] K.J. Cole, A.F. Carley, M.J. Crudace, M. Clarke, S.H. Taylor, G.J. Hutchings, Catal. Lett. 138 (2010) 143.
[21] K. Morgan, K.J. Cole, A. Goguet, C. Hardacre, G.J. Hutchings, N. Maguire, S.O. Shekhtman, S.H. Taylor, J. Catal. 276 (2010) 38.